

Cryo-EM structure of a metazoan separase–securin complex at near-atomic resolution

Andreas Boland, Thomas G Martin, Zigu Zhang, Jing Yang, Xiao-chen Bai, Leifu Chang, Sjors H W Scheres & David Barford

Separase is a caspase-family protease that initiates chromatid segregation by cleaving the kleisin subunits (Scc1 and Rec8) of cohesin, and regulates centrosome duplication and mitotic spindle function through cleavage of kendrin and Slk19. To understand the mechanisms of securin regulation of separase, we used single-particle cryo-electron microscopy (cryo-EM) to determine a near-atomic-resolution structure of the *Caenorhabditis elegans* separase–securin complex. Separase adopts a triangular-shaped bilobal architecture comprising an N-terminal tetratricopeptide repeat (TPR)-like α -solenoid domain docked onto the conserved C-terminal protease domain. Securin engages separase in an extended antiparallel conformation, interacting with both lobes. It inhibits separase by interacting with the catalytic site through a pseudosubstrate mechanism, thus revealing that in the inhibited separase–securin complex, the catalytic site adopts a conformation compatible with substrate binding. Securin is protected from cleavage because an aliphatic side chain at the P1 position represses protease activity by disrupting the organization of catalytic site residues.

The coordinated and accurate segregation of paired chromatids is critical to somatic cell division in mitosis and the genesis of germ cells in meiosis. Timely disjunction of coherent chromatids is achieved through the removal of centromeric cohesin, mediated by the separase-catalyzed proteolysis of the kleisin subunit of cohesin complexes^{1–3}. Accurate chromatid disjunction is crucial to prevent chromosome mis-segregation, which can contribute to aneuploidy and tumorigenesis^{4,5}. To ensure genome stability, separase activity is tightly regulated by binding to its inhibitory chaperone securin^{6–8}, a natively unfolded protein^{9,10} that is present in excess relative to separase in the cell and associates with separase during translation^{6–8,11}. Paradoxically, in addition to its inhibitory function, securin plays an important role in promoting separase activity^{12–14}. This is probably the result of stabilizing effects, as securin-deficient human HCT116 cells exhibit a roughly four-fold reduction in separase levels¹², and, conversely, overexpression of separase results in elevated levels of securin¹⁵. Stabilizing effects of securin on separase are also observed in other species, including the nematode *C. elegans*¹⁶. In vertebrates, a small proportion of separase activity is also inhibited through CDK-cyclin B1-dependent phosphorylation and binding^{15,17,18}. Separase activation is triggered by the anaphase-promoting complex (APC/C)-dependent ubiquitin-mediated proteolysis of securin and cyclin B1 (refs. 19–21).

Separase is a caspase-family protease comprising a C-terminal separase protease domain (SPD) with specificity for cleaving substrates C-terminal to an Arg residue (P1) within an (S/D)xExxR motif^{3,7,22}. In budding yeast, polo kinase-dependent phosphorylation of Scc1 (Pds1) at the Ser residue at P6 regulates Scc1 cleavage and thus sister-chromatid separation²³. A large N-terminal domain contributes to

securin and substrate interactions^{14,22,24}. Crystallographic studies of the SPD with inhibitory peptides explained the basis for substrate selection²⁵; however, the molecular mechanisms underlying separase regulation have not yet been defined.

To understand the dual mechanisms of activation and repression of separase activity by securin, we used single-particle cryo-EM to determine a near-atomic-resolution structure of the *C. elegans* separase–securin complex. We also determined a medium-resolution reconstruction of the human separase–securin complex, thus revealing the evolutionary conservation of separase's triangular shape. Our analyses provide insight into the overall architecture of separase, explain the substrate-occlusion inhibitory mechanism of securin, and rationalize the strict necessity of an arginine residue in the P1 binding pocket to mediate substrate-assisted cleavage. We also demonstrate the applicability of cryo-EM for the resolution of structures of macromolecules ~150 kDa in size that are difficult to crystallize.

RESULTS

Cryo-EM structure of separase–securin at 3.8-Å resolution

To optimize the contrast of a relatively small complex in cryo-electron micrographs, and to overcome the preferred molecular orientations of this complex encountered in vitreous ice, we used graphene-oxide-coated electron microscopy (EM) grids²⁶ (Supplementary Fig. 1). We determined a reconstruction of the asymmetric separase–securin complex at 3.8-Å resolution (Fig. 1, Table 1, and Supplementary Figs. 1 and 2). Most of the complex, particularly the larger separase subunit, was well defined in terms of EM density. Side chain density was unambiguously assigned for more than 95% of all structured

MRC Laboratory of Molecular Biology, Cambridge, UK. Correspondence should be addressed to A.B. (aboland@mrc-lmb.cam.ac.uk) or D.B. (dbarford@mrc-lmb.cam.ac.uk)

Received 18 January; accepted 6 February; published online 6 March 2017; doi:10.1038/nsmb.3386

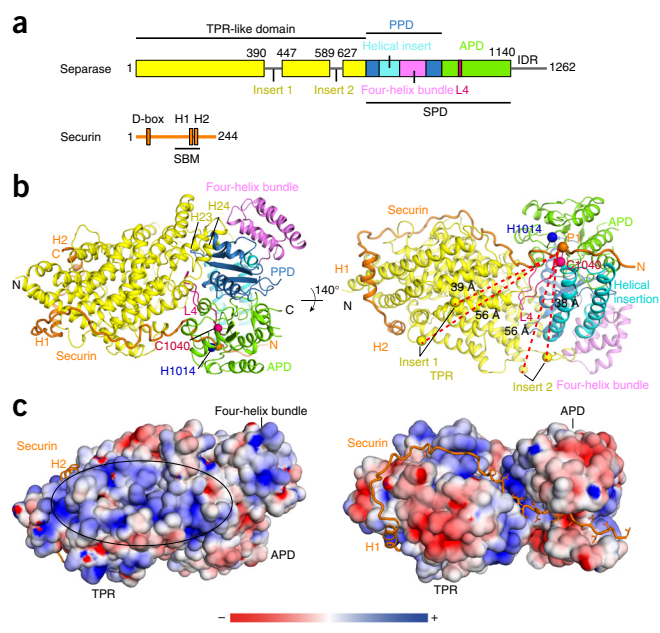


Figure 1 Overview of the *C. elegans* separase–securin complex. (a) Schematic of separase and securin. IDR, intrinsically disordered region. (b) Two views of the separase–securin complex. The catalytic site includes the catalytic dyad of His1014 and Cys1040, and the L4 loop. The positions of insert 1 and insert 2 relative to the catalytic site (corresponding to the C α atom of the P1 Met of securin) are shown as yellow spheres. The distances between the insert boundaries and the C α atom of the P1 residue of securin (Met126^{Sec}) are shown. (c) Two views of the molecular surface of separase, showing electrostatic potential, with securin in stick representation. The positively charged surface is outlined (left).

amino acids, which allowed complete *ab initio* model-building of separase. Securin, which forms an extended structure that interacts mainly with the periphery of separase, was well resolved around the substrate-binding site but less well defined elsewhere (Supplementary Fig. 2 and Table 1).

Overall architecture of the *C. elegans* separase–securin complex

The *C. elegans* separase–securin complex adopts a triangular-shaped bilobal architecture that measures 110 Å in its longest dimension and about 70 Å in its two other dimensions. Separase is composed of an N-terminal α -solenoid domain adjoined to the C-terminal SPD²⁵ (Fig. 1). A clearly defined cleft is situated at the interface of these two domains. The α -solenoid domain comprises 25 α -helices, mainly arranged as a right-handed superhelix that resembles a TPR superhelix, as predicted²⁷. In contrast to a canonical TPR superhelix, however, compression of the helix and the irregular length of its constituent α -helices create a compact globular structure that lacks the deep surface grooves typical of TPR proteins (Supplementary Fig. 3). The C terminus of the α -solenoid interacts with the SPD, whereas its N terminus is capped by securin, which could explain how securin contributes to separase stability^{12–14} (Figs. 1b and 2a). The α -solenoid domain accommodates two disordered insertions. Insert 1 includes the site of regulatory CDK phosphorylation of human separase^{17,28}, whereas insert 2 incorporates the autocleavage sites^{2,29,30} and the cyclin B1 (refs. 15,18) and PP2A³¹ binding sites of vertebrate separase (Fig. 1 and Supplementary Fig. 4). Both inserts project toward the separase catalytic site, located within reach of the tips of both inserts (Fig. 1b and Supplementary Fig. 4a,b).

Insert 2 of human separase is markedly longer than its counterpart in *C. elegans* separase, such that all three autocleavage sites are accessible to the catalytic site. The marked positive electrostatic potential on one surface of separase (Fig. 1c) might be related to its activation by DNA³² and the stimulation of Rec8 cleavage in meiosis by multi-site phosphorylation of Rec8, thus facilitating high-affinity binding of the substrate²⁷.

The SPD of *C. elegans* separase, like the *Chaetomium thermophilum* SPD (CtSPD)²⁵, is divided into two subdomains, one of which is the C-terminal active protease domain (APD) (Fig. 1a,b and Supplementary Fig. 5). The APD belongs to the caspase/gingipain family of cysteine proteases and incorporates an essential Cys–His catalytic dyad^{1,17,33}. The APD comprises a central β -sheet flanked on both sides by α -helices (Fig. 1b, left). The adjacent pseudoprotease domain (PPD) extends the APD β -sheet, in a manner reminiscent of the architecture of caspase dimers formed from active and inactive catalytic subunits³³. An α -helical insertion within the PPD stretches out over the PPD and the APD, forming extensive contacts with the APD (Fig. 1b, right). This long α -helical insertion is indispensable for protease activity, presumably because of its roles in substrate recognition, as discussed below, and in contributing to the structural integrity of the protein²⁵. It is followed by a four-helix bundle, which forms at the periphery of the APD (Fig. 1b, left).

Loop L4 conformation is constrained in the full-length protein

The SPD of the *C. elegans* separase–securin complex and the CtSPD²⁵ superimpose closely, with r.m.s. deviation of 3.5 Å over 365 C α atoms, and 1.6 Å over 121 C α atoms for the APD (Supplementary Fig. 5). The four-helix bundle is shifted in the *C. elegans* structure toward the N terminus of the molecule by 9 Å and is rotated by 7°. His1014^{Sep} and Cys1040^{Sep} of the catalytic dyad are located in loops L3 and L4, respectively (superscript labels “Sep” and “Sec” denote separase and securin residues, respectively). Caspases are regulated by the conformation of the L4 loop³³, and in the context of the securin–separase complex, the L4 loop adopts an active conformation, although the position of its tip differs from that of its counterpart in CtSPD²⁵ (Fig. 2).

The C terminus of the α -solenoid domain is capped by the SPD. An extensive hydrophobic interface is created primarily by docking of the H23 and H24 α -helices of the α -solenoid onto the central β -sheet of the PPD (Fig. 1b). Its large size suggests a stable interaction. The tip of the L4 loop projects into the groove of the α -solenoid superhelix (Fig. 2a,b). Phe1052^{Sep}, a conserved hydrophobic residue in separase (Supplementary Fig. 6), is located at the tip of L4 and is buried within a hydrophobic pocket of the α -solenoid domain (Fig. 2c). Mutations of the L4 loop in CtSPD modulate Scc1 cleavage rates²⁵, which shows that the conformation of the L4 loop contributes slightly to catalytic activity.

Securin acts as a noncleavable pseudosubstrate

Securin is an intrinsically disordered protein^{9,10} that functions as an inhibitory chaperone to both stabilize separase^{12–14} and, through a pseudosubstrate mechanism, inhibit protease activity^{14,29}. Our structure shows that when bound to separase, securin forms an extended conformation that interacts along the entire length of separase in an antiparallel orientation (Fig. 1b,c). The N-terminal 116 residues, including the APC/C degron recognition and ubiquitination sites, are unstructured (Fig. 1a). The separase-binding motif (SBM) encompasses residues 118–199 and is part of a previously identified inhibitory segment of securin³⁴ that is evolutionarily well conserved (Supplementary Fig. 7). The N terminus of the SBM blocks the separase catalytic site filling a 16-Å-wide cleft between the α -solenoid domain and the SPD (Figs. 1 and 2c). The SBM’s C terminus curls

Table 1 Data-processing statistics and model refinement

	<i>C. elegans</i> separase–securin (EMD-3583, PDB 5MZ6)	<i>Homo sapiens</i> separase–securin (EMD-3584)
Data collection		
Microscope	FEI Titan Krios	FEI Titan Krios
Voltage (kV)	300	300
Electron dose (e Å ⁻²)	40	40
Detector	Gatan K2 Summit	Gatan K2 Summit
Pixel size (Å)	1.43	1.05
Defocus range (μm)	1.0–3.0	1.0–3.0
Reconstruction (RELION)		
Particles	103,696	152,374
Box size (pixels)	180	240
Accuracy of rotations (°)	1.960	3.283
Accuracy of translations (pixels)	0.492	1.994
Map-sharpening <i>B</i> factor (Å ²)	–130	–
Final resolution (Å)	3.8	6.8
Model composition		
Protein residues	1,097	
Refinement		
Resolution (Å)	3.8	
FSC _{average}	0.82	
<i>R</i> factor	36.53	
R.m.s. deviation		
Bond length (Å)	0.007	
Bond angle (°)	1.012	
Validation		
Clashscore, all atoms	11.12	
Rotamer outliers (%)	0.57	
Ramachandran plot		
Favored (%)	93.73	
Allowed (%)	6.09	
Outliers (%)	0.18	
Disordered regions		
Separase	1–10, 391–446, 590–628, 894–899, 1,095–1,104, 1,141–1,262	
Securin	1–117, 193–244	
Side chains fitted (%)		
Separase (of ordered region)	96.3	
Securin (of ordered region)	84	

FSC, Fourier shell correlation.

along a hydrophobic path on the outside of the α -solenoid domain, with two short α -helices anchored within adjacent hydrophobic grooves (Figs. 1b,c and 2a). This is in agreement with biochemical studies indicating that the C terminus of securin contacts the α -solenoid domain of separase^{14,24}. A C-terminal fragment of the Scc1 substrate remains bound to separase even in the absence of the cleavage site residues²², which indicates the importance of the N-terminal α -solenoid domain in conferring high-affinity binding to both substrate and inhibitor.

Separase substrates share a common [D/E/S]xExxR motif (positions P6–P1) and are cleaved immediately C-terminal to the P1 Arg residue^{3,7,22} (Supplementary Fig. 7). Polo kinase phosphorylation of yeast Scc1 at the P6 serine stimulates separase cleavage²³. A DIExxΦ

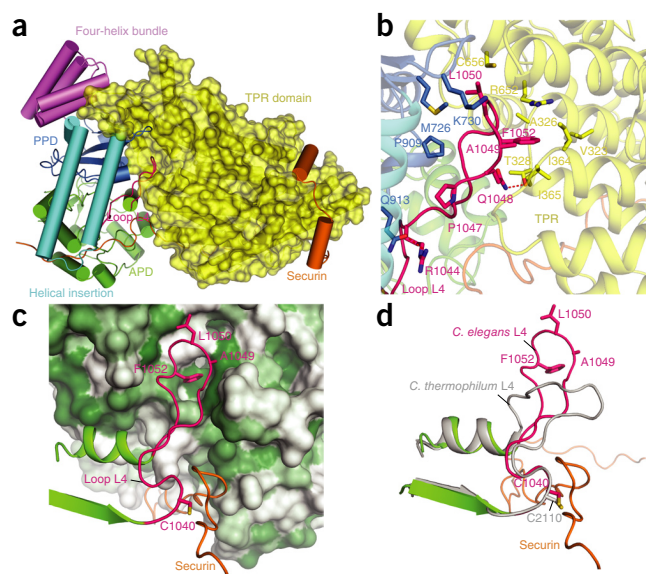


Figure 2 The α -solenoid domain stabilizes the L4 loop. (a) Overview of separase–securin, showing the molecular surface of the separase α -solenoid domain. (b) Details of the L4 loop's interactions with the α -solenoid domain. (c) View of the L4 loop docking into the L4-loop-binding pocket of the α -solenoid domain, shown as a hydrophobic surface color-coded from white to green to indicate increasing hydrophobicity. (d) The L4 loops of *C. elegans* SPD and *CtSPD* adopt an active conformation, with differences confined to the tip of the loop. Securin contacts the L4 loop.

motif in securin mimics substrate recognition, with the P1 Arg substituted by a hydrophobic residue (Met126^{Sec} in *C. elegans* securin)³⁴ (Supplementary Fig. 7). Notably, the P1 Arg of separase substrates is critical for cleavage^{7,22,35–37}. Replacing Arg with Ala, Asp or Glu eliminates proteolysis^{3,7,13,22}, whereas the securin pseudosubstrate motif is cleaved when an Arg is substituted for the hydrophobic residue at its P1-binding pocket^{25,34}.

Our structure reveals that the mode of interaction of the securin pseudosubstrate motif with *C. elegans* separase is remarkably similar to the interactions between the *CtSPD* and a covalently linked peptide mimicking Scc1 (Fig. 3a,b and Supplementary Fig. 8)²⁵. This confirms the concept that securin acts as a pseudosubstrate inhibitor^{14,29,34} and, importantly, indicates that in the inhibited *C. elegans* separase–securin complex, the separase catalytic site architecture adopts a conformation compatible with substrate recognition. In the *C. elegans* separase–securin complex, Ile122^{Sec} (P5) forms hydrophobic interactions with Phe783^{SEP}, a strictly conserved aromatic residue of the α -helical insert (Fig. 3c and Supplementary Fig. 6). This interaction rationalizes the strong conservation of residues with nonpolar character at the P5 site of separase substrates (Supplementary Fig. 7). Glu123^{Sec} at P4 forms electrostatic interactions with the highly conserved Arg1083^{SEP}, thus mimicking Scc1–*CtSPD* interactions²⁵. Amino acid side chains at variable positions P3 and P1' (ref. 22) are solvent exposed. C-terminal to the pseudosubstrate motif, securin inserts into the cleft that separates the SPD and the α -solenoid domain, contacting the L4 loop (Fig. 2a,c).

Similarly to the P1 Arg of the Scc1 peptide bound to *CtSPD*²⁵, Met126^{Sec} is anchored by the P1-binding pocket of *C. elegans* separase (Fig. 3c–e). This deep pocket is lined by a mixture of conserved hydrophobic and polar residues, including His1014^{SEP} of the catalytic dyad (Supplementary Fig. 6). Through conformational flexibility, the

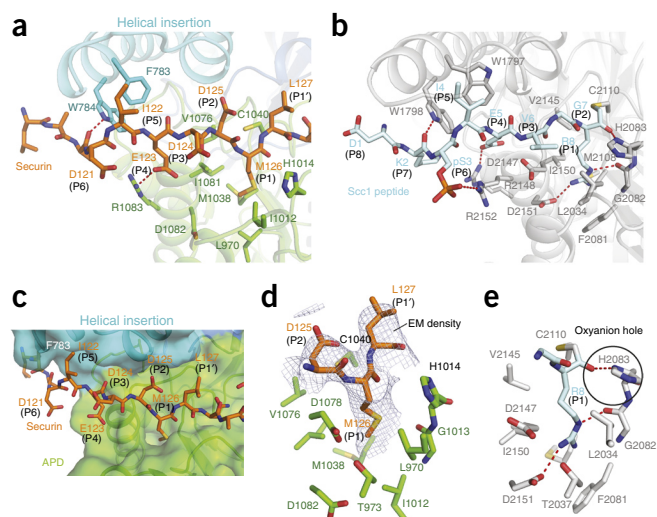


Figure 3 The interactions between the securin pseudosubstrate motif and separate resemble interactions with Scc1. **(a)** The securin pseudosubstrate motif at the *C. elegans* SPD. **(b)** Scc1-mimicking peptide at the CtSPD²⁵. **(c)** The molecular surface of *C. elegans* separase, showing the securin pseudosubstrate sequence engaging the peptide-substrate binding site of separate. **(d)** Details of the Met126 (P1) residue at the P1-binding site, and its corresponding EM density. **(e)** P1 Arg of the Scc1-mimicking peptide at the P1 site of CtSPD, showing the oxyanion hole formed from the catalytic His2083 (from ref. 25). The guanidinium side chain of the P1 Arg residue donates a hydrogen bond to the main chain carbonyl of Gly2082, positioning the imidazole side chain of His2083 to create the oxyanion hole and donate a hydrogen bond to the main chain carbonyl of Arg(P1). In contrast, Met126(P1) of *C. elegans* Scc1 widens the P1-binding pocket of *C. elegans* separase such that the main chain of Gly1012 and side chain of His1014 (equivalent to Gly2082 and His2083, respectively, of CtSPD) are displaced by ~2 Å.

P1 pocket accommodates both nonpolar residues of securin and the P1 Arg residue of separase substrates (**Fig. 3d,e** and **Supplementary Video 1**). Importantly, the interactions of an Arg side chain at the P1 pocket organize the configuration of catalytic site residues required for peptide cleavage. In the CtSPD structure, the invariant Asp2151 residue, equivalent to Asp1082^{SEP} that is rotated out of the P1-binding pocket in *C. elegans* separase, forms a stable bidentate salt bridge with the substrate P1 Arg guanidinium group²⁵ (**Fig. 3e**). This interaction allows the Nε atom of the P1 Arg guanidinium group to donate a hydrogen bond to the main chain carbonyl of Gly2082^{SEP} that orients the catalytic His2083^{SEP} side chain to create the oxyanion hole for the carbonyl oxygen at P1 (**Fig. 3e**). In the *C. elegans* separase–securin complex, the P1-binding pocket widens to accommodate the nonpolar Met126^{Sec} side chain. Relative to their counterparts in CtSPD, Gly1013^{SEP} and the imidazole ring of His1014^{SEP} move away from Met126^{Sec} by almost 2 Å (**Fig. 3d** and **Supplementary Fig. 8a,b**). Thus, an Arg at P1 functions to mediate catalysis by orienting the catalytic His to create the oxyanion hole, necessary for cleavage of the scissile bond^{1,17}.

The triangular shape of separase is conserved throughout evolution

Although the SPD is conserved across eukaryotes (**Supplementary Fig. 5**), sequence similarities within the α-solenoid domain are difficult to discern (**Supplementary Fig. 4c**). However, we can confirm that the triangular shape of separase–securin is evolutionarily conserved, because the structure of *C. elegans* separase–securin is similar to a medium-resolution cryo-EM reconstruction of the human

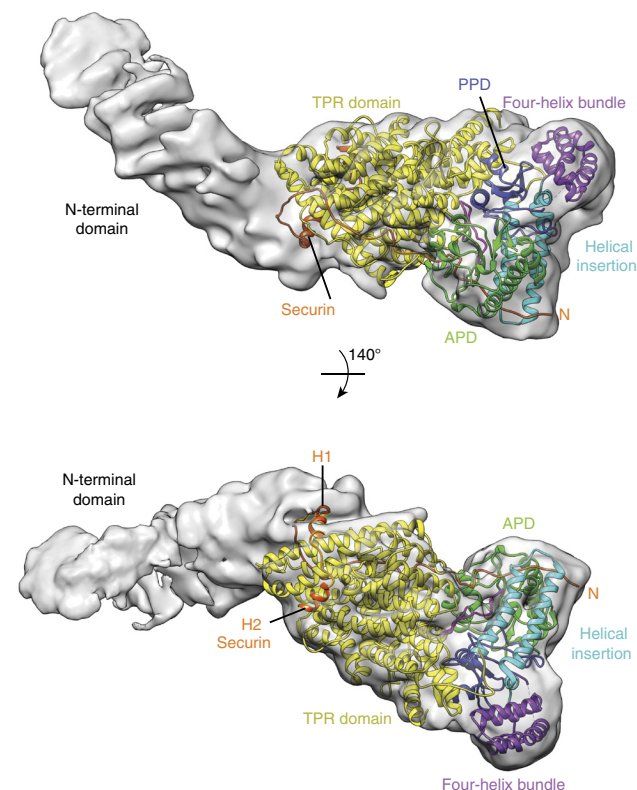


Figure 4 Cryo-EM reconstruction of the human separase–securin complex. Shown are two views of the cryo-EM density as a transparent molecular envelope, with the coordinates of *C. elegans* separase–securin fitted to the map as a rigid body. Structures are color-coded as in **Figure 1**.

complex (**Fig. 4** and **Supplementary Fig. 1**), and consistent with a previous negative-stain EM reconstruction²⁴. *C. elegans* separase–securin resembles the ‘whale’-like domain described in the human separase–securin structure²⁴. The flexible ‘tail’-like feature at the N terminus of human separase–securin is not present in our structure of the *C. elegans* complex. This probably represents the N-terminal 650 residues of human separase²⁷ that are absent from *C. elegans* (**Supplementary Fig. 4**). A recently reported EM structure of *C. elegans* separase–securin complex at 24-Å resolution¹⁶ revealed a bilobal architecture that has similar overall dimensions to and is generally compatible with our cryo-EM structure, despite the lower resolution and use of negative stain.

DISCUSSION

The substrate Arg P1 residue that participates in organizing the catalytic site has a role that is reminiscent of those of other enzymes that derive specificity through substrate-assisted catalysis^{38,39}. It explains the requirement for an Arg at P1 for substrate cleavage^{3,7,22}, and why securin is capable of engaging the separase substrate-binding site, in competition with Scc1, without itself being cleaved²². Thus, securin inhibits separase through a competitive mechanism that interferes with substrate recognition, and represses its intrinsic protease activity through small conformational rearrangements of its catalytic site. This inhibition mechanism contrasts with XIAP’s inhibition of caspases, in which XIAP blocks access to the substrate-binding cleft by binding in the reverse orientation^{40,41}.

Here we have shown how securin inhibits separase through a substrate-occlusion mechanism. Additionally, securin destruction and displacement from the TPR lobe may promote a conformational

change of separase that affects the catalytic site and L4 loop that stimulates catalytic activity. Future structural studies of securin-free separase are required to address this question, and also to elucidate other regulatory mechanisms, including the mutually exclusive CDK1–cyclin B1-dependent repression of vertebrate separase that involves a phospho-dependent Pin1-catalyzed peptidyl prolyl *cis/trans*-isomerization²⁸, leading to cyclin B1 association and separase inhibition.

Mutation, overexpression or mislocalization of separase leads to an elevated incidence of tumor development^{42,43}, and thus inhibition of separase is a tempting pharmacological target. This structure will provide a rational molecular basis for the design of small-molecule drugs to inhibit uncontrolled separase activity in certain cancer types.

METHODS

Methods, including statements of data availability and any associated accession codes and references, are available in the [online version of the paper](#).

Note: Any Supplementary Information and Source Data files are available in the [online version of the paper](#).

ACKNOWLEDGMENTS

This work was funded by the Medical Research Council (MC_UP_1201/6 to D.B., and MC_UP_A025_1013 to S.H.W.S.), a Cancer Research UK grant (C576/A14109 to D.B.), Long Term EMBO Fellowships (ALTF 79-2014 to A.B., and ALTF 1229-2013 to T.G.M.) and H2020 Marie-Curie Fellowships (657725 to A.B., and 657990 to T.G.M.). We thank members of the Barford group for helpful discussions; T. Tischer for helpful suggestions and support; C. Savva, S. Chen and G. McMullan for maintaining EM facilities; J. Grimmett and T. Darling for computing; and P. Emsley for constant support with COOT. We acknowledge Diamond for access and support of the cryo-EM facilities at the UK national electron bio-imaging centre (eBIC), proposal EM13708, funded by the Wellcome Trust, MRC and BBSRC.

AUTHOR CONTRIBUTIONS

Z.Z. cloned the separase–securin constructs used in this study. A.B. and J.Y. generated the wild-type and mutant separase–securin viruses, respectively. A.B. established the protein purifications. A.B. and T.G.M. prepared grids and collected EM data, with contributions from X.-c.B. and L.C. A.B. analyzed EM data and determined the 3D reconstructions, aided by T.G.M. and S.H.W.S. A.B. and D.B. built the model *ab initio* and made the figures. D.B. directed the project and designed experiments with A.B. A.B. and D.B. wrote the manuscript, with input from all other authors.

COMPETING FINANCIAL INTERESTS

The authors declare no competing financial interests.

Reprints and permissions information is available online at <http://www.nature.com/reprints/index.html>.

- Uhlmann, F., Wernic, D., Poupart, M.A., Koonin, E.V. & Nasmyth, K. Cleavage of cohesin by the CD clan protease separin triggers anaphase in yeast. *Cell* **103**, 375–386 (2000).
- Waizenegger, I.C., Hauf, S., Meinke, A. & Peters, J.M. Two distinct pathways remove mammalian cohesin from chromosome arms in prophase and from centromeres in anaphase. *Cell* **103**, 399–410 (2000).
- Hauf, S., Waizenegger, I.C. & Peters, J.M. Cohesin cleavage by separase required for anaphase and cytokinesis in human cells. *Science* **293**, 1320–1323 (2001).
- Santaguida, S. & Amon, A. Short- and long-term effects of chromosome mis-segregation and aneuploidy. *Nat. Rev. Mol. Cell Biol.* **16**, 473–485 (2015).
- Kamenz, J. & Hauf, S. Time to split up: dynamics of chromosome separation. *Trends Cell Biol.* **27**, 42–54 (2017).
- Ciosk, R. *et al.* An ESP1/PDS1 complex regulates loss of sister chromatid cohesion at the metaphase to anaphase transition in yeast. *Cell* **93**, 1067–1076 (1998).
- Uhlmann, F., Lottspeich, F. & Nasmyth, K. Sister-chromatid separation at anaphase onset is promoted by cleavage of the cohesin subunit Scc1. *Nature* **400**, 37–42 (1999).
- Zou, H., McGarry, T.J., Bernal, T. & Kirschner, M.W. Identification of a vertebrate sister-chromatid separation inhibitor involved in transformation and tumorigenesis. *Science* **285**, 418–422 (1999).
- Sánchez-Puig, N., Veprintsev, D.B. & Fersht, A.R. Human full-length securin is a natively unfolded protein. *Protein Sci.* **14**, 1410–1418 (2005).
- Csizmok, V., Felli, I.C., Tompa, P., Banci, L. & Bertini, I. Structural and dynamic characterization of intrinsically disordered human securin by NMR spectroscopy. *J. Am. Chem. Soc.* **130**, 16873–16879 (2008).
- Hellmuth, S. *et al.* Positive and negative regulation of vertebrate separase by Cdk1-cyclin B1 may explain why securin is dispensable. *J. Biol. Chem.* **290**, 8002–8010 (2015).
- Jallepalli, P.V. *et al.* Securin is required for chromosomal stability in human cells. *Cell* **105**, 445–457 (2001).
- Nagao, K., Adachi, Y. & Yanagida, M. Separase-mediated cleavage of cohesin at interphase is required for DNA repair. *Nature* **430**, 1044–1048 (2004).
- Hornig, N.C., Knowles, P.P., McDonald, N.Q. & Uhlmann, F. The dual mechanism of separase regulation by securin. *Curr. Biol.* **12**, 973–982 (2002).
- Holland, A.J. & Taylor, S.S. Cyclin-B1-mediated inhibition of excess separase is required for timely chromosome disjunction. *J. Cell Sci.* **119**, 3325–3336 (2006).
- Bachmann, G. *et al.* A closed conformation of the *Caenorhabditis elegans* separase–securin complex. *Open Biol.* **6**, 160032 (2016).
- Stemmann, O., Zou, H., Gerber, S.A., Gygi, S.P. & Kirschner, M.W. Dual inhibition of sister chromatid separation at metaphase. *Cell* **107**, 715–726 (2001).
- Gorr, I.H., Boos, D. & Stemmann, O. Mutual inhibition of separase and Cdk1 by two-step complex formation. *Mol. Cell* **19**, 135–141 (2005).
- Cohen-Fix, O., Peters, J.M., Kirschner, M.W. & Koshland, D. Anaphase initiation in *Saccharomyces cerevisiae* is controlled by the APC-dependent degradation of the anaphase inhibitor Pds1p. *Genes Dev.* **10**, 3081–3093 (1996).
- Funabiki, H. *et al.* Cut2 proteolysis required for sister-chromatid separation in fission yeast. *Nature* **381**, 438–441 (1996).
- Yamamoto, A., Guacci, V. & Koshland, D. Pds1p, an inhibitor of anaphase in budding yeast, plays a critical role in the APC and checkpoint pathway(s). *J. Cell Biol.* **133**, 99–110 (1996).
- Sullivan, M., Hornig, N.C., Porstmann, T. & Uhlmann, F. Studies on substrate recognition by the budding yeast separase. *J. Biol. Chem.* **279**, 1191–1196 (2004).
- Alexandru, G., Uhlmann, F., Mechtler, K., Poupart, M.A. & Nasmyth, K. Phosphorylation of the cohesin subunit Scc1 by Polo/Cdc5 kinase regulates sister chromatid separation in yeast. *Cell* **105**, 459–472 (2001).
- Viadiu, H., Stemmann, O., Kirschner, M.W. & Walz, T. Domain structure of separase and its binding to securin as determined by EM. *Nat. Struct. Mol. Biol.* **12**, 552–553 (2005).
- Lin, Z., Luo, X. & Yu, H. Structural basis of cohesin cleavage by separase. *Nature* **532**, 131–134 (2016).
- Pantelic, R.S., Meyer, J.C., Kaiser, U., Baumeister, W. & Plitzko, J.M. Graphene oxide: a substrate for optimizing preparations of frozen-hydrated samples. *J. Struct. Biol.* **170**, 152–156 (2010).
- Katis, V.L. *et al.* Rec8 phosphorylation by casein kinase 1 and Cdc7-Dbf4 kinase regulates cohesin cleavage by separase during meiosis. *Dev. Cell* **18**, 397–409 (2010).
- Hellmuth, S. *et al.* Human chromosome segregation involves multi-layered regulation of separase by the peptidyl-prolyl-isomerase Pin1. *Mol. Cell* **58**, 495–506 (2015).
- Waizenegger, I., Giménez-Abián, J.F., Wernic, D. & Peters, J.M. Regulation of human separase by securin binding and autocleavage. *Curr. Biol.* **12**, 1368–1378 (2002).
- Zou, H., Stemman, O., Anderson, J.S., Mann, M. & Kirschner, M.W. Anaphase specific auto-cleavage of separase. *FEBS Lett.* **528**, 246–250 (2002).
- Holland, A.J., Böttger, F., Stemmann, O. & Taylor, S.S. Protein phosphatase 2A and separase form a complex regulated by separase autocleavage. *J. Biol. Chem.* **282**, 24623–24632 (2007).
- Sun, Y. *et al.* Separase is recruited to mitotic chromosomes to dissolve sister chromatid cohesion in a DNA-dependent manner. *Cell* **137**, 123–132 (2009).
- McLuskey, K. & Mottram, J.C. Comparative structural analysis of the caspase family with other clan CD cysteine peptidases. *Biochem. J.* **466**, 219–232 (2015).
- Nagao, K. & Yanagida, M. Securin can have a separase cleavage site by substitution mutations in the domain required for stabilization and inhibition of separase. *Genes Cells* **11**, 247–260 (2006).
- Buonomo, S.B. *et al.* Disjunction of homologous chromosomes in meiosis I depends on proteolytic cleavage of the meiotic cohesin Rec8 by separin. *Cell* **103**, 387–398 (2000).
- Sullivan, M., Lehane, C. & Uhlmann, F. Orchestrating anaphase and mitotic exit: separase cleavage and localization of Slk19. *Nat. Cell Biol.* **3**, 771–777 (2001).
- Matsuo, K. *et al.* Kendrin is a novel substrate for separase involved in the licensing of centriole duplication. *Curr. Biol.* **22**, 915–921 (2012).
- Keusekotten, K. *et al.* OTULIN antagonizes LUBAC signaling by specifically hydrolyzing Met1-linked polyubiquitin. *Cell* **153**, 1312–1326 (2013).
- Wickliffe, K.E., Lorenz, S., Wemmer, D.E., Kuriyan, J. & Rape, M. The mechanism of linkage-specific ubiquitin chain elongation by a single-subunit E2. *Cell* **144**, 769–781 (2011).
- Huang, Y. *et al.* Structural basis of caspase inhibition by XIAP: differential roles of the linker versus the BIR domain. *Cell* **104**, 781–790 (2001).
- Riedl, S.J. *et al.* Structural basis for the inhibition of caspase-3 by XIAP. *Cell* **104**, 791–800 (2001).
- Zhang, N. *et al.* Overexpression of separase induces aneuploidy and mammary tumorigenesis. *Proc. Natl. Acad. Sci. USA* **105**, 13033–13038 (2008).
- Mukherjee, M. *et al.* Overexpression and constitutive nuclear localization of cohesin protease Separase protein correlates with high incidence of relapse and reduced overall survival in glioblastoma multiforme. *J. Neurooncol.* **119**, 27–35 (2014).

ONLINE METHODS

Cloning and expression of *C. elegans* and *Homo sapiens* genes related to the separase–securin complex. The cDNAs encoding the *C. elegans* and *H. sapiens* separase and securin genes were ordered as gene-optimized versions for expression in insect cells, and synthesized cDNAs (GeneArts/Thermo Fisher) were subsequently cloned into pU1 (separase) and pF1 (securin) vectors⁴⁴. A double StrepII tag followed by a TEV (tobacco etch virus) site was fused N-terminal to the separase gene. An N-terminal truncation of 139 residues of *C. elegans* securin was generated by mutagenesis PCR, and a TEV-cleavable MBP tag was added C-terminal to securin in the human construct. The resultant plasmids were transformed into MultiBacDH10 α Cre cells to generate bacmids through *in vivo* recombination⁴⁴. A single recombinant vector was used for recombinant baculovirus generation.

Separase–securin overexpression. Recombinant P3 baculoviruses were used to infect High Five insect cells (Invitrogen) at a cell density of roughly 2.0×10^6 cells per ml. The cells were incubated for 72 h at 27 °C at 150 r.p.m., harvested at a cell viability rate of ~80%, flash-frozen in liquid nitrogen and stored at –80 °C.

Purification of separase–securin complexes. Purification of the protein complexes was performed at 4 °C. Cells were resuspended in lysis buffer (50 mM Tris-HCl, pH 8.3, 250 mM NaCl, 1 mM EDTA, 1 mM DTT, protease inhibitor cocktail tablets (Complete EDTA-free; Roche Diagnostics GmbH), 0.1 mM PMSF, 5 units/ml benzonase (Novagen)), sonicated, and centrifuged for 1 h at 48,000g. The soluble fraction was slowly (1 ml/min flow rate) applied to a 5-ml StrepTactin Superflow Cartridge (Qiagen) and washed with wash buffer (lysis buffer without protease inhibitor cocktail, PMSF and benzonase) until stable UV absorption could be observed. Peak fractions were incubated with TEV protease at 4 °C overnight, and wash buffer without NaCl (buffer A) was used for a two-fold dilution before loading onto a ResourceQ anion-exchange column (GE Healthcare) the next day. After a washing step, the complexes were eluted with a gradient of buffer B (20 mM Tris-HCl, pH 8.0, 1 M NaCl, 1 mM DTT). A final size-exclusion step on a Superose 6 Increase 10/300 GL column with 20 mM HEPES-NaOH, pH 7.8, 200 mM NaCl and 1 mM DTT was performed.

Preparation of graphene-oxide-support-covered grids. A graphene oxide dispersion (Sigma-Aldrich; 2 mg/ml in H₂O) was diluted ten-fold with ddH₂O to a final concentration of 0.2 mg/ml and subsequently spun down at 300g for ~15 s to remove large aggregates of graphene oxide flakes (pellet formation could be observed occasionally) (as described in ref. 26). After incubation for 1 min with graphene oxide dispersion, Quantifoil grids were glow-discharged for 1 min with an Edwards Sputter Coater S150B. After incubation, the graphene oxide solution was removed by brief blotting with Whatman No. 1 filter paper and washed by absorbance of 20 μ l of ddH₂O onto the graphene-oxide-coated side twice and once on the back side of the grid, with blotting steps in between (for a detailed video and protocol, see https://figshare.com/articles/Graphene_Oxide_Grid_Preparation/3178669). The tendency of biological molecules to adopt preferred orientations in thin vitreous ice probably results from interactions at the hydrophobic air-water interface. Presumably these interactions favor the largest exposed hydrophobic surface and thus select specific molecular orientations. Immobilization of the sample on a carbon, graphene or graphene oxide support substrate reduces interactions at the air-water interface. In contrast to the air-water interface, graphene oxide is hydrophilic, and thus will interact with different surfaces of separase–securin, thus promoting different orientations.

Electron microscopy data collection. Purified separase–securin complexes from *C. elegans* and *H. sapiens* were applied to graphene-oxide-covered gold 300 square mesh Quantifoil R1.2/1.3 holey carbon grids (Quantifoil Micro Tools GmbH) at a concentration of ~100 nM (waiting time, 30 s; blotting time, 8 s) and flash-frozen in liquid ethane, using a custom-fabricated manual plunger at 4 °C. *C. elegans* separase specimens were imaged manually on an FEI Titan Krios electron microscope operating at 300 kV accelerating voltage. Zero-energy-loss micrographs were recorded with a Gatan K2 Summit direct electron detector executed in super-resolution counting mode at the end of a Gatan GIF Quantum energy filter with a slit width of 20 eV. The calibrated magnification was 34,965, corresponding to a pixel size of 1.43 Å, and images were collected at a dose rate of ~2.5 electrons/Å²/s. Exposures (16 s each) were dose-fractionated into 20 movie

frames with a total dose of ~40 electrons per Å². Defocus values in the final data set ranged from –1.0 to –3.3 μ m. Automated data acquisition with the same exposure time and total dose as described for the *C. elegans* separase–securin complex was used for data collection of the human separase–securin complex at Diamond Light Source with a calibrated magnification of 47,619, corresponding to a pixel size of 1.05 Å.

Image processing. Super-resolution micrograph movies with a pixel size of 0.715 Å were binned to 1.43 Å. Micrograph movie frame stacks were first aligned with MOTIONCORR⁴⁵ before further processing. The contrast transfer function parameters were determined with GCTF⁴⁶, and RELION⁴⁷ was used for most other image-processing steps. Initial particle picking was done with e2boxer.py in EMAN2 (ref. 48), using only a subset of the data set, and particles were extracted with a 180-pixel by 180-pixel box. Reference-free 2D classification yielded initial 2D classes that were subsequently used as references (a low-pass filter of 20 Å was applied to avoid reference bias) for automatic particle picking⁴⁹. A high-pass filter of 400 Å with a 50-Å width of the raised cosine on the high-pass filter edge was applied to all micrographs to correct for the ice gradient present on most of the micrographs, in order to reduce false positive picking of particles. In total, 2.4 million particles were picked from 2,793 micrographs and extracted from original unmodified micrographs. Iterative reference-free two-dimensional class averaging and strict selection of classes that showed distinct/strong structural features resulted in a particle subset of 665,331 particles. An *ab initio* 3D reconstruction was created with SIMPLE-PRIME⁵⁰ and used as an initial model for a first 3D refinement. Correction of beam-induced motion of individual particles and B-factor weighting of single frames to treat radiation damage problems were done in the particle-polishing step⁵¹ in RELION. Auto-refinement of polished particles with a soft mask (with 5-pixel fall-off) around the entire molecule led to a density map of 4.2-Å resolution. This particle subset was subjected to two rounds of 3D classifications to separate structural heterogeneity and dispose of remaining bad particles (**Supplementary Fig. 9**). In a final step, all micrographs with a resolution of >4.0 Å according to the resolution estimation of GCTF were discarded, which resulted in a final data set of 103,696 particles that refined to a map with a resolution of 3.8 Å. All resolution estimations were derived from Fourier shell correlation (FSC) calculations between reconstructions from two independently refined half-sets, and reported resolutions are based on the FSC = 0.143 criterion^{52,53}. Local resolution was estimated with ResMap⁵⁴. Images collected at the Diamond Light Source were collected in counting mode and processed as described for the *C. elegans* data set, with the exception of a 240-pixel \times 240-pixel box size, owing to the larger particle size. Auto-refinement of particles with a soft mask (with 5-pixel fall-off) around the entire molecule led to a density map of 6.8-Å resolution. It is likely that this resolution is overestimated owing to the strong preferred orientation of the particles.

Model-building and refinement of the *C. elegans* separase–securin complex. *Ab initio* modeling of the entire *C. elegans* separase–securin complex was performed in COOT⁵⁵. A recently published crystal structure of the C-terminal lobe of the *C. thermophilum* separase²⁵ was fitted into the density with Chimera⁵⁶ and used as a template and validation tool for modeling the SPD. The final model of separase lacks the N-terminal ten residues, two long unstructured loop regions (insert 1 and insert 2) present in the α -solenoid domain (residues 391–446 and residues 590–626), and the C-terminal 122 residues that are predicted to be unstructured and for which no density could be observed. The model was refined with Refmac v.5.8 (ref. 57) and PHENIX⁵⁸. Secondary structure restraints were created by PROSMART⁵⁹.

Structure-based sequence alignment of separase TPR domains. The N-terminal sequence of human separase (residues 1–1,692, N-terminal to the SPD) was analyzed for predicted secondary structure elements and disordered regions with PHYRE2 (ref. 60). This indicated an α -helical segment interspersed with two predicted disordered regions (residues 1,070–1,040 and 1,307–1,561). The positions of these two disordered regions approximately matched those of insert 1 and insert 2 of *C. elegans* separase (residues 390–442 and 597–618). Residues 1–390 of *C. elegans* separase were aligned with residues 651–1,070 of human separase, on the basis of matching of predicted α -helices of human separase with observed α -helices of *C. elegans* separase, and also guided by a published multiple sequence alignment of part of the N-terminal domain of separase²⁷. Residues

442–597 and 618–700 of *C. elegans* separase aligned with residues 1,140–1307 and 1,561–1641 of human separase, respectively. The multiple sequence alignment in **Supplementary Figure 4** was generated using ALSCRIPT⁶¹.

Data availability. EM maps for the securin–separase complexes have been deposited in the EMDB with accession codes EMD-3583 (*C. elegans*) and EMD-3584 (*H. sapiens*). Atomic coordinates for *C. elegans* separase–securin have been deposited in the PDB with accession code 5MZ6. Other data and materials related to this paper are available on request.

44. Zhang, Z., Yang, J. & Barford, D. Recombinant expression and reconstitution of multiprotein complexes by the USER cloning method in the insect cell-baculovirus expression system. *Methods* **95**, 13–25 (2016).
45. Li, X. *et al.* Electron counting and beam-induced motion correction enable near-atomic-resolution single-particle cryo-EM. *Nat. Methods* **10**, 584–590 (2013).
46. Zhang, K. Gctf: real-time CTF determination and correction. *J. Struct. Biol.* **193**, 1–12 (2016).
47. Scheres, S.H. RELION: implementation of a Bayesian approach to cryo-EM structure determination. *J. Struct. Biol.* **180**, 519–530 (2012).
48. Tang, G. *et al.* EMAN2: an extensible image processing suite for electron microscopy. *J. Struct. Biol.* **157**, 38–46 (2007).
49. Scheres, S.H. Semi-automated selection of cryo-EM particles in RELION-1.3. *J. Struct. Biol.* **189**, 114–122 (2015).
50. Elmlund, H., Elmlund, D. & Bengio, S. PRIME: probabilistic initial 3D model generation for single-particle cryo-electron microscopy. *Structure* **21**, 1299–1306 (2013).
51. Scheres, S.H. Beam-induced motion correction for sub-megadalton cryo-EM particles. *eLife* **3**, e03665 (2014).
52. Scheres, S.H. & Chen, S. Prevention of overfitting in cryo-EM structure determination. *Nat. Methods* **9**, 853–854 (2012).
53. Rosenthal, P.B. & Henderson, R. Optimal determination of particle orientation, absolute hand, and contrast loss in single-particle electron cryomicroscopy. *J. Mol. Biol.* **333**, 721–745 (2003).
54. Kucukelbir, A., Sigworth, F.J. & Tagare, H.D. Quantifying the local resolution of cryo-EM density maps. *Nat. Methods* **11**, 63–65 (2014).
55. Emsley, P. & Cowtan, K. Coot: model-building tools for molecular graphics. *Acta Crystallogr. D Biol. Crystallogr.* **60**, 2126–2132 (2004).
56. Yang, Z. *et al.* UCSF Chimera, MODELLER, and IMP: an integrated modeling system. *J. Struct. Biol.* **179**, 269–278 (2012).
57. Murshudov, G.N. *et al.* REFMAC5 for the refinement of macromolecular crystal structures. *Acta Crystallogr. D Biol. Crystallogr.* **67**, 355–367 (2011).
58. Adams, P.D. *et al.* PHENIX: building new software for automated crystallographic structure determination. *Acta Crystallogr. D Biol. Crystallogr.* **58**, 1948–1954 (2002).
59. Nicholls, R.A., Fischer, M., McNicholas, S. & Murshudov, G.N. Conformation-independent structural comparison of macromolecules with ProSMART. *Acta Crystallogr. D Biol. Crystallogr.* **70**, 2487–2499 (2014).
60. Kelley, L.A., Mezulis, S., Yates, C.M., Wass, M.N. & Sternberg, M.J. The Phyre2 web portal for protein modeling, prediction and analysis. *Nat. Protoc.* **10**, 845–858 (2015).
61. Barton, G.J. ALSCRIPT: a tool to format multiple sequence alignments. *Protein Eng.* **6**, 37–40 (1993).